Astron. Astrophys. 353, 944–951 (2000)

ASTRONOMY AND ASTROPHYSICS

Luminosity function and mass segregation in M92

G. Andreuzzi[1], **R. Buonanno**[1], **F. Fusi Pecci**[2], **G. Iannicola**[1], **and G. Marconi**[1]

[1] Astronomical Observatory of Rome, via di Frascati 33, 00040 Monteporzio Catone, Roma, Italy (gloria@coma.mporzio.astro.it)
[2] Astronomical Observatory of Bologna, via Zamboni 33, 40126 Bologna, Italy

Received 26 May 1999 / Accepted 27 October 1999

Abstract. We present WFPC2-HST observations of the lower main sequence of the galactic globular cluster M92 (NGC6341), extending down to V $\simeq$ 27. Our data, which cover a region of the cluster extending from the very center out to r $\simeq$ 380 arcsec, show that the slope of the luminosity function becomes flatter going towards the center of the cluster, as expected if M92 is a dynamically relaxed system.

The slope of the inferred power-law mass function we computed ranges from x $\simeq$ 0.7 for the field centered at r = 18.61 core radii, to x $\simeq$ 0.3 for the annular field centered at r = 10.61 core radii, where a value of 14 arcsec has been used for the core radius of M92. Such a result, obtained without making any use of dynamical theoretical models, shows that segregation effects are at work in M92.

Key words: Galaxy: globular clusters: individual: M92 – stars: low-mass, brown dwarfs – stars: luminosity function, mass function

1. Introduction

The Hubble Space Telescope (HST) now makes it possible to obtain color-magnitude diagrams and luminosity functions of globular clusters extending several magnitudes fainter than the Main Sequence turn off. Insight into the formation and dynamical history of globular clusters can be obtained from the radial dependence of the mass function, or comparing the mass functions of clusters with different physical characteristics (i.e. metallicity, position in the galaxy, central density, etc.).

Galactic globular clusters, in particular, appear to be the best suited environments in which to investigate the contribution of low-mass stars to the dark halos in galaxies because they retain the memory of the unevolved stellar initial mass function (IMF). In fact globular cluster stars fainter than the Main Sequence Turn-off (MS-TO) are substantially unevolved and are located along the MS according to their initial mass. Their luminosity distribution is usually described by the Initial Mass Function as modified by subsequent dynamical evolution to become the so-called Present Day Mass Function (PDMF). In any case the stellar counts are a unique probe of the MF in globulars and in addition they allow us to infer the existence of extremely low-mass objects.

Arguably, the observed mass function of a cluster depends on its metallicity, its orbit in the Galaxy and dynamical history and is therefore correlated with the origin and the evolution of the cluster (McClure et al. 1986; Aguilar et al. 1988; Djorgovski et al. 1993). In particular McClure et al. (1986), found that the slope of the mass function increases from -0.75 in 47 Tuc to -2.06 in M15, a result which they interpreted as evidence that the mass function strongly depends on metallicity. This conclusion was confirmed, although somewhat weakened by Pryor et al. (1986) who applied theoretically derived radial mass segregation corrections to the data set of McClure et al. More recently Piotto et al. (priv. comm.) and Carretta et al. (priv. comm.), comparing different clusters, found evidence of marginal dependence of the MF slopes from the metallicity.

Given the importance of these issues, we performed the WFPC2-HST photometry of the metal-poor, high-concentration galactic globular cluster M92 which, as the archetype of metal-poor globulars, has been the object of several studies in the past (see Stetson et al. 1988; Heasley et al. 1986; Johnson & Bolte 1998, for ground-based photometry, and Piotto et al. 1997 for HST photometry). Table 1 lists the central density, core radius, metallicity, distance modulus and reddening for M92.

The main objectives of this study were: a) to locate the lower main sequence in the more central regions of the cluster with greater accuracy than in previous studies and b) to compare deep LFs for two adjacent fields extending from $\simeq$ 100 arcsec to $\simeq$ 380 arcsec from the center of M92.

Sects. 2 and 3 present the data, the reduction procedures and the CMDs obtained for the four chips of the WFPC2. The re-

Table 1.

Physical parameters for M92		
$\log\rho_0$ $(\mathrm{M}_\odot/\mathrm{pc}^3)$	4.4	Djorgovski & Meylan (1993)
$\log r_c$ (arcsec)	1.15	Djorgovski & Meylan (1993)
$[Fe/H]$	-2.15	Gratton et al. (1997)
$(\mathrm{m}-\mathrm{M})_0$	14.61	Pont et al., (1997)
	14.74	Gratton et al (1997)
$\mathrm{E(B-V)}$	0.025	Gratton et al (1997)

Send offprint requests to: G. Andreuzzi

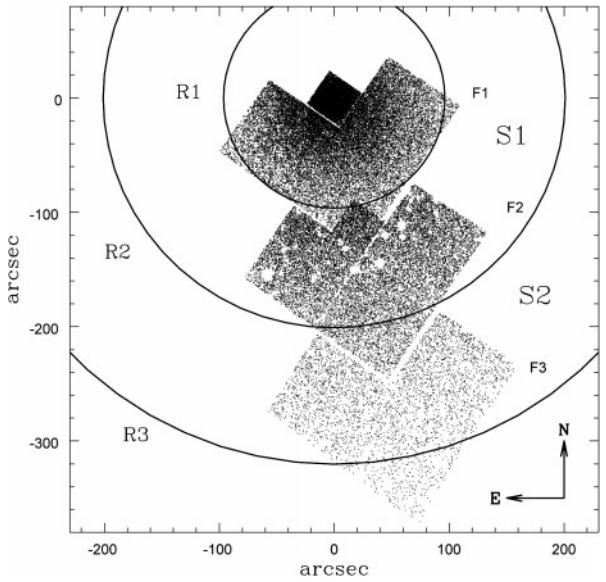

Fig. 1. Plot of the locations of the three HST-WFPC2 fields in M92.

Table 2. Journal of observations for fields F1 (internal), F2 (middle) and F3 (external). N is the number of exposures; t(s) is the exposure times in seconds.

INTERNAL			MIDDLE			EXTERNAL		
filter	N	t(s)	filter	N	t(s)	filter	N	t(s)
F555W	6	70	F555W	2	500	F555W	2	700
	4	2		2	600		1	300
F814W	6	100	F814W	2	400	F814W	2	400
	4	1.2		2	700		2	500

Table 3. Detected stars in the three observed WFPC2 mosaic fields. N is the total number of stars in each field; V_{lim} is the magnitude limit of the stars (4 σ above the background).

FIELD	N	$V_{\rm lim}$
F1	30852	25
F2	16444	27.5
F3	3848	27.5

sulting LFs are presented and discussed in Sect. 4, while the resulting MFs are discussed in Sect. 5. Final results are summarized in Sect. 6.

2. Observations and reductions

The HST + WFPC2 observations were obtained within the framework of the program GO 5969, carried out on December 3, 1995. The observations consisted of three fields, F1, F2 and F3 located at 96.2, 200.9 and 320.3 arcsec respectively from the cluster center. The location of the fields are as follows (see Fig. 1): the center of the Planetary Camera (0.046 arcsec/pixel) of field 1 is placed at the center of the cluster in such a way that the outer quarter of the Wide Field detector WF3 (0.0996 arcsec/pixel) overlaps the Planetary Camera of field 2, while the outer part of the detector WF3 of field 2 overlaps the Planetary Camera of field 3. Consequently the other two detectors WF2 and WF4 map two regions, located at a radial distance intermediate between PC and WF3, respectively westwards and eastwards of WF3. This spatial coverage allowed us to obtain an homogeneous calibration from the very center of the cluster out to the more external regions of F3. The corresponding exposures are listed in Table 2.

Corrections to the raw data for bias, dark and flat-fielding were performed using the standard HST pipeline. Subsequent data reduction was made using MIDAS routines and the Romafot package for crowded fields (Buonanno et al., priv. comm.).

First, a filter median was applied to each frame using software in ROMAFOT in order to remove cosmic rays from single frames. Then, since lower MS stars are cool and red, we used the deepest I image to search for stellar objects in each chip.

All the objects identified in this search were fitted in all I and V frames using a PSF profile modelled by a Moffat function, plus a numerical map of the residuals, to better take into account the contribution of the stellar wings. The identified candidates were then measured on each individual V and I frame, and an average instrumental magnitude was derived for each object in each colour.

Table 3 reports the number of stars detected and measured in each field. These stars are plotted in Fig. 1 where three circles have been outlined in order to select two regions, S1 and S2, at significantly different radial distances. From the cluster center, the radius of each circle is, respectively, R1 $\simeq$ 96 arcsec, corresponding to about 7 core radii, R2 $\simeq$ 200 arcsec, corresponding to 14 core radii, and R3 $\simeq$ 320 arcsec, corresponding to 22 core radii.

Inspection of Table 3 reveals that photometry in the external fields (F2 and F3) goes much fainter than that in F1, reflecting only in part the difference of the exposure times. As it is arguable that the higher degree of crowding in F1 prevented the photometry of the faintest stars, we decided to limit the present study to the deep LFs of fields F2 and F3, and to postpone the study of the bright portion of the LF of the internal field F1 to a forthcoming paper.

The tables with the x,y coordinates, V magnitudes and V-I colors, can be obtained via Internet from host 'coma.mporzio.astro.it' using the 'anonymous ftp' service (directory, /pub/M92).

The instrumental magnitudes were transformed into the standard Johnson system following Holtzman et al. (1995).

3. Color-magnitude diagrams

The I, V-I CMDs for the fields F2 and F3, are shown in Fig. 2 and Fig. 3 respectively, where the mean errors per interval of magnitude are indicated.

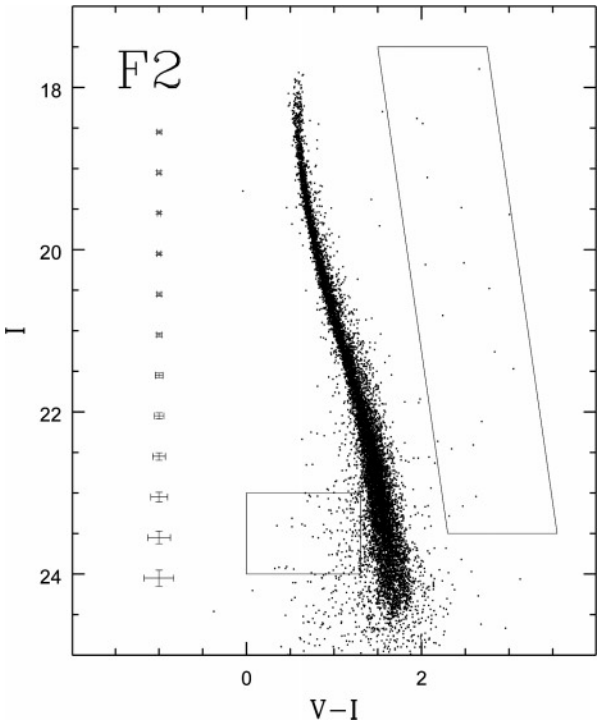

Fig. 2. V-I colour-magnitude diagram for the field F2. The bars reported in the figure represent the mean errors at the given magnitude. The parallelograms in the figure select red and blue outliers (see text for details).

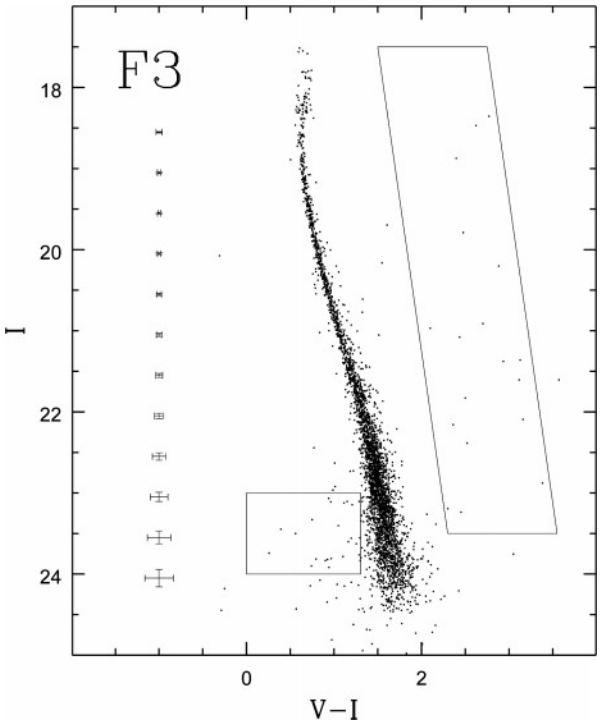

Fig. 3. V-I colour-magnitude diagram for the field F3, as in Fig. 2

These errors were estimated through the rms frame-to-frame scatter for each star with the average error in each magnitude bin computed using the relation:

$$\sigma = \frac{1}{N_S}\sum_{k=1}^{N_S}\left[\frac{\sum_{i=1}^{N_f}(V_i - < V >)^2}{N_f}\right]^{1/2}$$

where N_f is the number of frames, N_S is the number of stars in the interval, V_i are the magnitudes, and $< V >$ is the mean magnitude of each star averaged over the frames where that star has been measured.

From inspection of Fig. 2 and Fig. 3 one notices four important features. First, the main sequence of the inner field appears wider than that of the outer field, second, the number of blue outliers is correspondingly larger in F2 than in F3, third, both the fields present a few tens of red outliers, and finally, both the sequences are not sharply defined towards the red colors, although a genuine parallel to the main sequence doesn't appear clearly in the diagrams.

In order to have insight into all these questions, we computed the ridge line applying an iterative procedure which consisted in dividing the sample into bins 0.5 mag wide and computing the median V-I color in steps of 0.02 mag. Then, all the objects lying more than 3 σ from the median were rejected and the procedure of computing the median was iterated until the result turned out to be stable.

Table 4. Standard deviations and internal errors for the fields F2 and F3 per interval of magnitude. N is the number of stars in each bin.

$I \pm 0.25$	N(F3)	σ(F3)	Σ(F3)	N(F2)	σ(F2)	Σ(F2)
18.550	43	0.035	0.034	203	0.027	0.044
19.050	68	0.011	0.033	346	0.022	0.044
19.550	110	0.011	0.033	499	0.020	0.054
20.050	151	0.014	0.047	640	0.024	0.055
20.550	168	0.021	0.072	902	0.027	0.070
21.050	171	0.025	0.074	828	0.032	0.084
21.550	231	0.030	0.072	973	0.043	0.085
22.050	319	0.039	0.075	1217	0.054	0.085
22.550	540	0.061	0.081	1735	0.071	0.089
23.050	701	0.081	0.091	1894	0.095	0.108
23.550	590	0.106	0.119	1583	0.129	0.130
24.050	454	0.123	0.149	1195	0.168	0.159

As second step we estimated the spread of the main sequence by computing the standard deviation, Σ_i, of the color histograms of the main sequence in bins of 0.5 mag. We list in Table 4 the Σ_i and the internal errors, σ_i, separately for the two field F2 and F3.

Inspection of Table 4 reveals that, excluding the first bin, both the average internal error and the observed spread of the main sequence are always larger in F2 than in F3 and that both of them are correlated with the number N of stars in each bin. This correlation clearly indicates that the photometric accuracy decreases with the degree of image crowding which is larger in the inner field, F2. A second problem which arises from inspec-

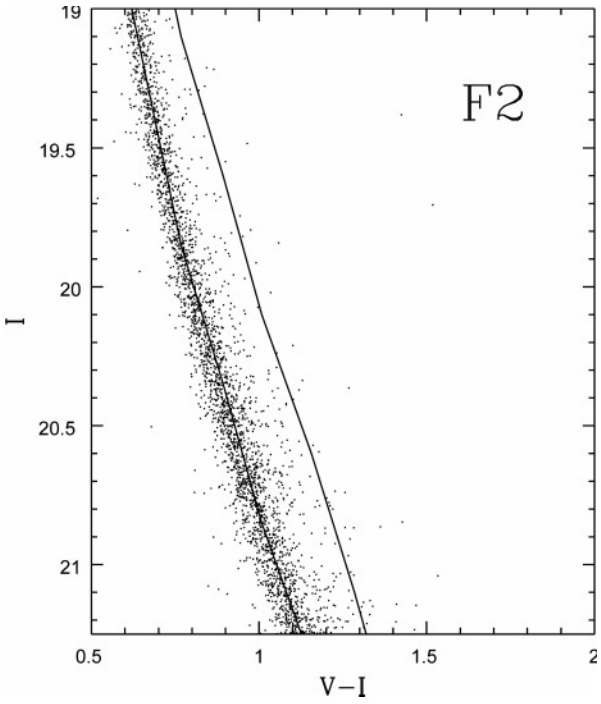

Fig. 4. V-I colour-magnitude diagrams for the field F2. The superimposed lines are the ridge line and a line shifted of 0.75 mag in I respect to the ridge line.

tion of Table 4 is that the computed errors do not account for the dispersion actually observed along the main sequence, in fact the data in Columns 4 and 7 are systematically larger than those in Columns 3 and 6.

Likely the origin of this problem is in part due to the asymmetry, towards the red colours, of the distribution of the stars on the main sequence in both the fields F2 and F3, a feature which is usually interpreted as due to the presence of binaries. In fact, under the simplified assumption that most of the observed binaries consist of stars of nearly equal mass, one should expect that the binaries lie on a sequence shifted by 0.75 mag with respect to the main sequence. This effect is obviously observable only if the main sequence is not vertical in the CMD. Therefore we plotted in Fig. 4 the slanting portion of the CMD for field 2 with a parallel sequence 0.75 mag brighter. A simple inspection of this figure reveals that most of the red objects lie below the 0.75 mag line which is compatible with a binary hypothesis.

The last two features in the CMDs we noted refer to the blue and red outliers.

Concerning the red outliers, we simply counted the objects lying in the parallelogram, sketched both in Fig. 2 and Fig. 3, which defines a region of the CMD far enough from the main sequence locus of M92, and found 19 and 18 objects respectively in F2 and F3. Considering that the Galactic model of Bahcall et al. (1990) predicts that 21 stars with $(V-I) > 1$ and $15 < I < 23$ should fall in field 2 and field 3, we conclude that the red outliers in Fig. 2 and Fig. 3 are likely foreground stellar images.

The last feature of interest in Fig. 2 and Fig. 3 is the blue plume of objects fainter than I $\simeq$ 23. In this case the model of Bahcall et al. (1990) turns out to be less useful because 68 background objects (galaxies + stars) are predicted between I=23 and I=24, a number which, by inspection of Fig. 2, appears higher than is that observed. Therefore we chose to rely on observations and simply counted the objects falling in an area defined by the strips $23 < I < 24$ and $0 < (V-I) < 1.3$ finding 20 objects in the external field F3 and a figure six times larger in the correspondent area of the internal field F2. It is certainly unrealistic to imagine that the number of background galaxies could present such strong fluctuations on scales of a hundred arcseconds, we concluded therefore that the presence of the blue outliers is due to some artifact of the higher number of objects in F2 than in F3. This seems to be actually the case if one considers that the average color of the blue plume is $(V-I) \simeq 0.75$, i.e. roughly the same color of the stars in the brighter portion of the main sequence. We suggest in conclusion that photometry of the faint stars in Fig. 2 has been affected by the wings of images of the brighter stars and that therefore, a large portion of the blue outliers are genuine faint main sequence stars.

4. The luminosity function

The correction for incompleteness (i.e. the fraction of stars presumably lost because of crowding) was estimated as a function of I magnitude using the procedure based on selected real stars (Buonanno et al., priv. comm.). The real stars were added randomly to the I frames used for the original search of stellar peaks, paying attention to add just a few percent (≤ 10 %) of the total number of stars actually present in the frame, to avoid a significant enhancement of the image crowding.

The data reduction process described in Sect. 2 was then repeated from the peak detection phase to the profile fitting, obtaining positions and instrumental magnitudes for all the objects.

As a basic criterium, if a star in the output file was found to coincide ($\Delta X, \Delta Y < 1.5$ pixel, $\Delta mag < 0.3$) with the star input values, it was added to the number of recovered objects (N_{rec}). We considered recovered only those stars that did not migrate into the adjacent bins. The ratio $N_{rec}/N_{add}=\Phi$, the completeness factor, was then derived through a minimum of 10 trials for each bin of magnitude, then taking an average over each bin.

The luminosity function is shown in Fig. 5 and listed in Table 5a,b where the actual counts, the completeness factor and the counts corrected for this factor are reported for each chip and for the two fields. The absolute magnitudes of Column 1 have been obtained adopting $(m-M)_V$=14.82, E_{B-V}=0.025 (Gratton et al. 1997), $E_{V-I} = 1.24 E_{B-V}$ (Cardelli et al. 1988) and, then, $(m-M)_I$=14.77.

The luminosity functions of Fig. 5 present the same characteristic already found in other galactic globular clusters with a maximum at $M_I \simeq 8.3$ and a slow decrease to fainter luminosities (De Marchi & Paresce 1995a, b; Piotto et al. 1997, Marconi et al. 1998, and references therein). It is, therefore, natural to investigate whether the effect of a radial dependence of the luminosity function, already observed in several globular clusters, is

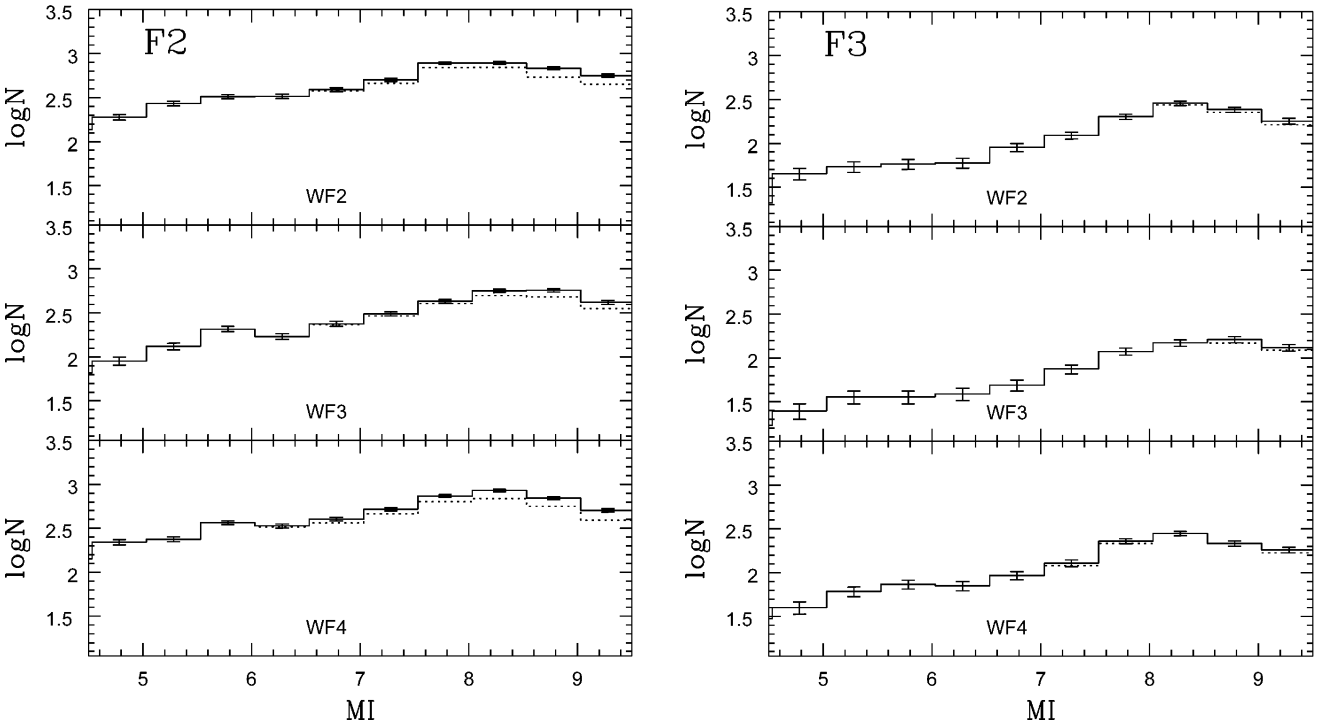

Fig. 5. Observed luminosity functions for the three separate cameras (WF2, WF3, WF4) in bins of 0.5 mag (solid lines). The error bars reflect Poisson error only and the dashed lines show the LFs before of correcting for completeness.

Table 5. Left (a): Luminosity functions for the WF2, WF3 and WF4 in the I band in 0.5 mag bin in the field F2. Right (b): the same for field F3. N is the actual number of stars observed; Φ is the completeness factor in each bin; N_C is the number of stars after the corrections for incompleteness have been applied.

F2	WF2			WF3			WF4		
M_I	N	Φ	N_C	N	Φ	N_C	N	Φ	N_C
3.03–3.53	58	1.00	58	7	1.00	7	10	1.00	10
3.53–4.03	92	1.00	92	43	1.00	43	68	1.00	68
4.03–4.53	136	1.00	136	66	1.00	66	143	1.00	143
4.53–5.03	189	1.00	189	90	1.00	90	220	1.00	220
5.03–5.53	271	1.00	271	132	1.00	132	238	1.00	238
5.53–6.03	325	1.00	325	208	1.00	208	367	1.00	367
6.03–6.53	327	1.00	327	171	1.00	171	330	0.98	337
6.53–7.03	375	0.96	390	234	0.98	239	364	0.89	404
7.03–7.53	462	0.91	503	291	0.94	308	465	0.88	521
7.53–8.03	690	0.87	780	405	0.94	429	638	0.84	740
8.03–8.53	700	0.88	784	500	0.87	565	693	0.77	852
8.53–9.03	541	0.74	682	482	0.81	573	563	0.76	698
9.03–9.53	449	0.75	561	354	0.82	418	392	0.71	506

F3	WF2			WF3			WF4		
M_I	N	Φ	N_C	N	Φ	N_C	N	Φ	N_C
3.03–3.53	16	1.00	16	7	1.00	7	18	1.00	18
3.53–4.03	15	1.00	15	11	1.00	11	17	1.00	17
4.03–4.53	21	1.00	21	17	1.00	17	30	1.00	30
4.53–5.03	45	1.00	45	25	1.00	25	40	1.00	40
5.03–5.53	54	1.00	54	36	1.00	36	61	1.00	61
5.53–6.03	58	1.00	58	36	1.00	36	74	1.00	74
6.03–6.53	60	1.00	60	39	1.00	39	71	1.00	71
6.53–7.03	90	1.00	90	49	1.00	49	93	1.00	93
7.03–7.53	123	1.00	123	75	1.00	75	121	0.94	128
7.53–8.03	202	1.00	202	119	1.00	119	216	0.94	229
8.03–8.53	273	0.95	287	149	1.00	149	281	1.00	281
8.53–9.03	226	0.93	242	148	0.90	163	216	1.00	216
9.03–9.53	163	0.90	179	123	0.93	132	168	0.92	181

found in the present set of data which cover a significant interval of radial distance.

We therefore produced the LFs listed in Table 6 for the stars in the two annular rings shown in Fig. 1 whose average distances from the center of the cluster are respectively $r_{S1} \simeq 149$ arcsec (2.2 half-light radius; hereinafter R_{h_L}) and $r_{S2} \simeq 261$ arcsec (4.0 R_{h_L}). The last column of Table 6, which reports the number of background galaxies expected on the basis of the estimates of Bahcall et al. (1990), reveals that faint galaxies are always a small fraction of the counts, apart from the second last of the bins where they are estimated to be about the 30 % of the cluster stars in the external field. The counts in the last bin, although reported, will be ignored in the rest of the paper, as they have a large uncertainty.

The luminosity functions for S_1 and S_2, after applying corrections for incompleteness and for statistical decontamination of background galaxies, have been normalized to the number of stars in the peak and are shown in Fig. 6.

Inspection of this figure reveals that the two LFs have similar shapes, but considerably different slopes, in the sense that the

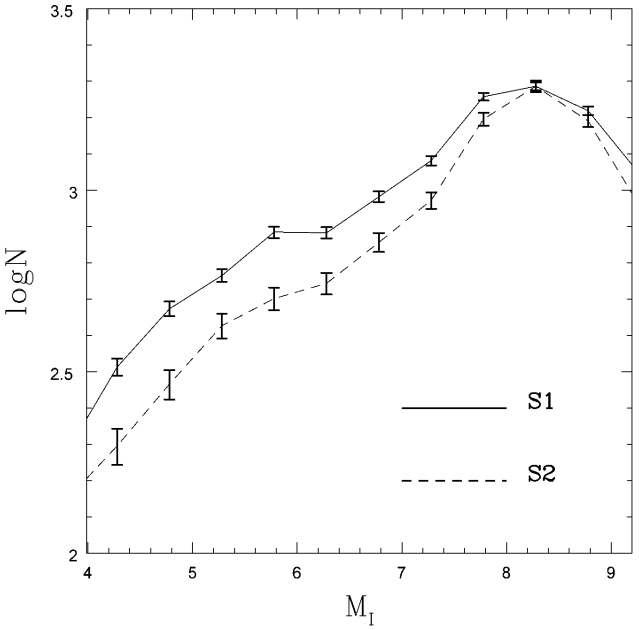

Fig. 6. Observed luminosity functions for the two fields S1 (solid line) and S2 (dashed line) in bins of 0.5 mag, normalized to the peak (M_I=8.28).

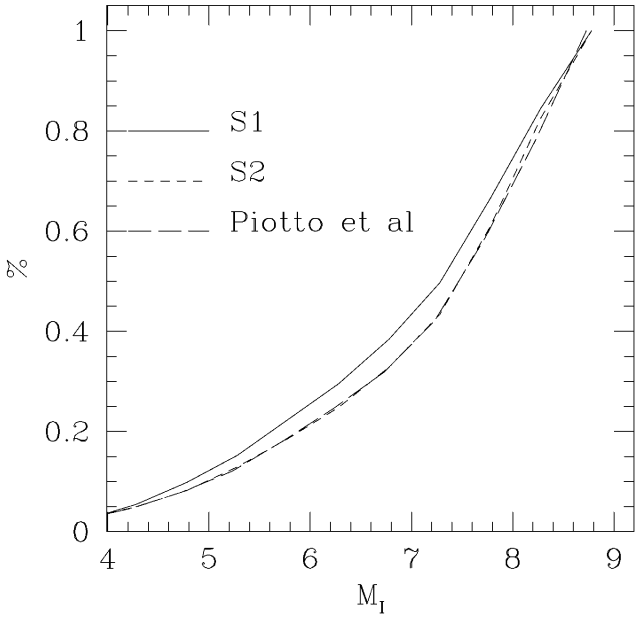

Fig. 7. Integrated luminosity functions for our two fields S1 and S2 and for Piotto's field. The distributions have been normalized to the integral of stars below M_I = 8.78.

Table 6. Luminosity functions for the fields S1 and S2 in the I band in 0.5 mag bins. N is the actual number of stars; Φ is the completeness factor; N_{gal} is the expected number of background galaxies.

	S1		S2		
M_I	N	Φ	N	Φ	N_{gal}
3.03–3.53	72	1.00	41	1.00	0.00
3.53–4.03	186	1.00	54	1.00	0.00
4.03–4.53	326	1.00	77	1.00	0.00
4.53–5.03	472	1.00	114	1.00	0.00
5.03–5.53	582	1.00	165	1.00	0.00
5.53–6.03	767	1.00	196	1.00	0.00
6.03–6.53	756	0.99	216	1.00	0.00
6.53–7.03	893	0.92	280	1.00	0.00
7.03–7.53	1110	0.89	378	0.97	20.0
7.53–8.03	1600	0.85	619	0.97	21.0
8.03–8.53	1686	0.82	791	0.97	46.0
8.53–9.03	1367	0.75	645	0.96	52.0
9.03–9.53	967	0.73	468	0.91	128.
9.53–10.03	390	0.35	104	0.65	155.0

ratio between the bright and the faint stars is larger in S1 than in S2, in qualitative agreement with the dynamical modifications that stars in globular clusters experience as a consequence of the energy equipartition due to two-body relaxation (Spitzer 1987). The Kolmogorov-Smirnov test indicates that the two LFs are different at the 99.981 % level, in the interval $M_I \simeq [4.3 - 8.3]$. An interesting check is to compare the LF in S2 with that derived by Piotto et al. (1997) in a different field of M92 at almost the same radial distance of S2. This comparison, shown in Fig. 7 where the integral distributions of the stars in S1, S2 and in Piotto's field have been reported, confirms that the LFs derived at the same radial distance are indistinguishable and that both of them are clearly different from the LF derived in the region S1.

5. The mass function

One of the most important pieces of information contained in the deep LFs of globular clusters is the number of low mass stars in the cluster. Unfortunately an empirical mass-luminosity relation for low-metallicity stars is nearly impossible to derive and on the theoretical side, a definitive mass-luminosity relation (MLR) has not yet been calculated given the lack of observational constraints.

This situation is particularly frustrating if one considers that the MFs for low-mass stars turn out to depend more on the adopted mass-luminosity relation than on the observed features of the LFs (see Ferraro et al. 1997 for a discussion). With all these cautions and considering that for metallicities of the order of $Z \simeq 10^{-4}$ even the most recent calculations do not satisfactorily reproduce the observed LFs (Silvestri et al. 1998), we have converted our LFs into MFs using several MLRs available in the literature (e.g. Montalban et al. (priv. comm.), MDM99; Baraffe et al. 1997, BCAH97; Alexander et al. 1997, AL97) as well as new models provided by Cassisi et al. (priv. comm., CCC99). We found that all the adopted MLRs reproduce quite well the location and the slope of the main sequence of M92, shown in Fig. 8, when the distance modulus and reddening derived by Gratton et al. (1997) is adopted.

Fig. 9 shows the MFs for the two fields S1 and S2 derived using the relation of BCAH97; the two MFs have been normalized in such a way to have the first bins (M=0.73 $M_\odot$) coincident. Clearly both the MFs show a similar behaviour, increasingly

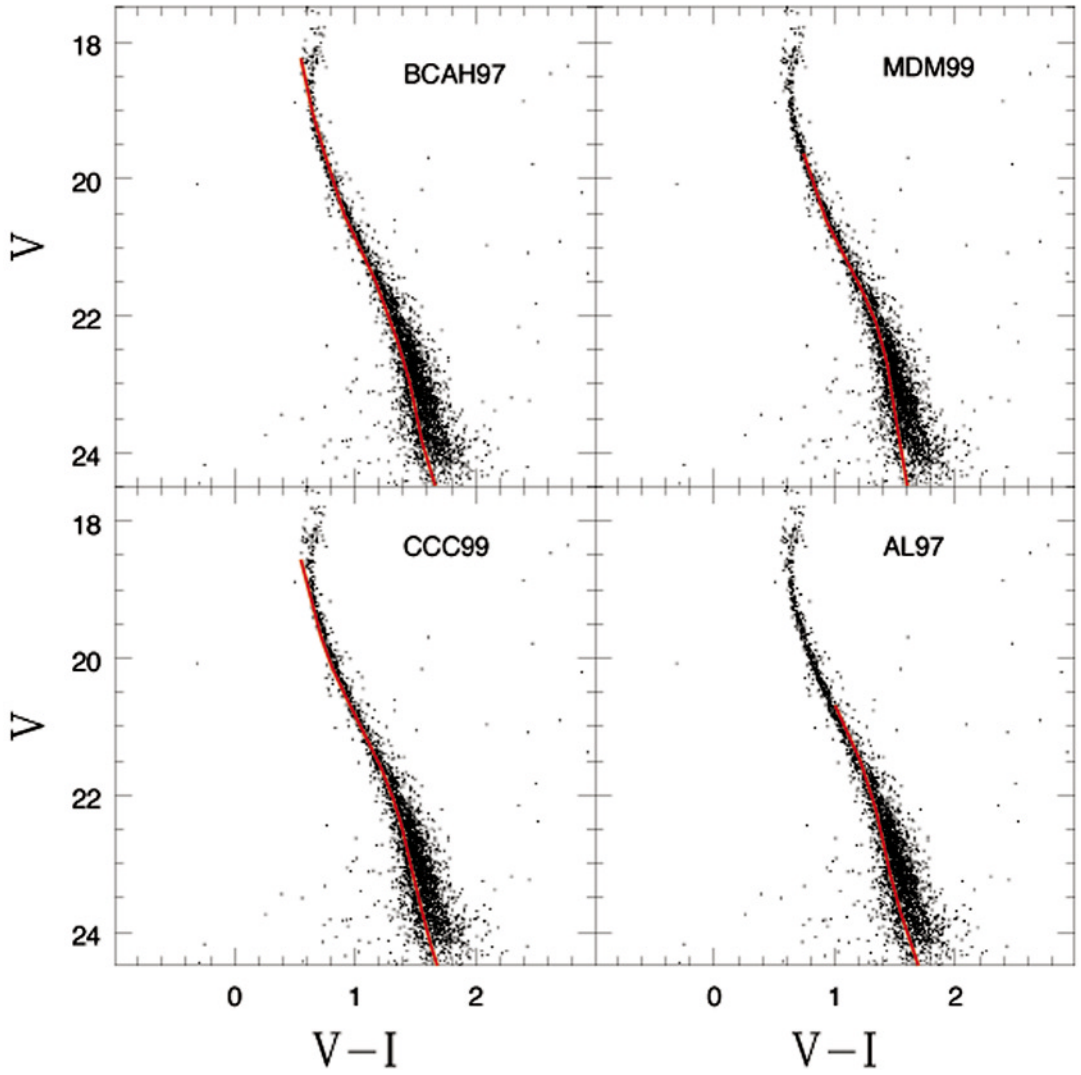

Fig. 8. Comparison of our M92 color-magnitude diagram with theoretical models from: BCAH97 ([Fe/H] = -2.0); MDM99 ([Fe/H] = -2.0); AL97 ([Fe/H] = -2.3); CCC99 ([Fe/H] = -2.0).

monotonically from 0.73 $M_\odot$ to a peak at 0.26 $M_\odot$. The error bars come only from counting statistics in each bin and do not include any 'theoretical error' from the MLR.

We emphasized that neither MF is well fit by a single power law over the entire range of masses. In any case adopting a power law of the form

$$\Phi(M)dM \propto M^{-(1+x)}dM \quad (1)$$

for masses in the range $0.73\ M_\odot \leq M \leq 0.26 M_\odot$, we derived an average slope x $\simeq$ 0.27 for the field S1 and $\simeq$ 0.71 for the field S2. If the upper end of the main sequence ($M \geq 0.4 M_\odot$) is ignored (then we considered only the linear part of the MFs), the observed MFs can be reasonably well fit by a power law with slopes $x_1 \simeq 0.6$ for field S1 and $x_2 \simeq 1$ for field S2, respectively. Note that the value we derive for S2 is in excellent agreement with the value derived by Piotto et al. (1997) for the field located at the same distance from the cluster center.

All considered, we conclude that there exists an appreciable difference between the two MFs, as expected from mass segregation effects.

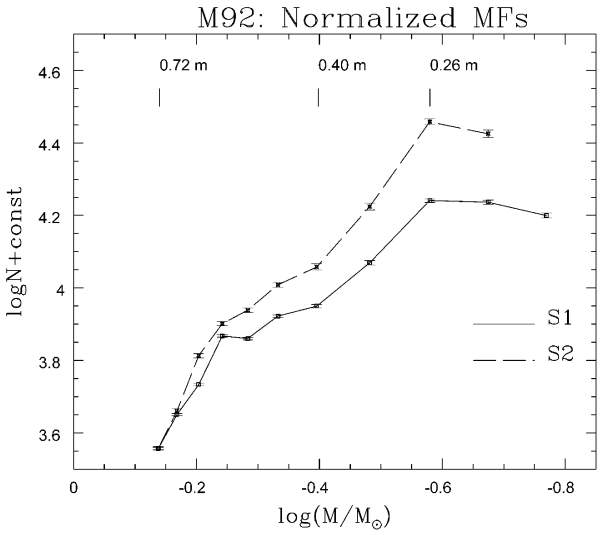

Fig. 9. Radial Mass functions obtained from the LFs of Fig. 6 in the fields S1 and S2 of M92. The adopted mass-luminosity relation is that of BCAH97 for a metallicity of [Fe/H]=-2.0.

A second result is that the slopes we derived, for stars below $\simeq 0.7 M_{\odot}$, are always flatter than the Salpeter MF in the low mass regime (Tinney, 1999). By comparing these slopes with that derived for the disk MF (x $\simeq$ 1, Mera et al. 1996), and with that derived for the field stars (x $\simeq$ 0.3, Kroupa et al. 1993, Kroupa 1995; x $\simeq$ -0.1, Gould et al. 1997), we concluded that they represent an upper limit for the Present Day Mass Function for both field stars and globular clusters. Similar results have been recently reported by Piotto et al. (priv. comm.) for a sample of globular clusters.

6. Summary

We have presented new V, I deep HST photometry of two fields in M92 reaching down to V $\simeq$ 27.5. The main results of this study are the following:

1) The asymmetry of the main sequence suggests that an unresolved sequence of few binary stars exists in our CMDs.

2) The slope of the LFs (and MFs) changes with the radial distance from the cluster center, suggesting that significant mass segregation has taken place in M92.

3) We found that the mass function in the interval $0.26 \leq M/M_{\odot} \leq 0.73$ is described by a power law with average exponent $x(r) \simeq 0.3 - 0.7$. It should be emphasized, however, that this value, although similar to that found for other metal-poor clusters (Piotto et al. 1997), and larger than that derived for metal rich clusters (Bolte 1987), relies on the MLR for low-mass, low-metallicity stars and is therefore too uncertain to draw any conclusion on the dependence of the MF with the metallicity.

Acknowledgements. It is our pleasure to thank S. Cassisi and F. D' Antona for providing us the tabulated theoretical MLRs and for helpful suggestions. We also warmly thank M. Limongi A. Chieffi, L. Pulone, H. B. Richer and M. Castellani for useful discussions, comments and suggestions. The support of the MURST is gratefully acknowledged.

References

Aguilar L., Hut P., Ostriker J.P., 1988, ApJ 335, 720
Alexander D.R., Brocato E., Cassisi S., et al., 1997, A&A 317, 90 (AL 97)
Bahcall J.N., Guhathakurta P., Schneider D.P., 1990, Sci 248, 178
Baraffe I., Chabrier G., Allard F., Hauschildt P.H., 1997, A&A 327, 1054 (BCAM 97)
Bolte M., 1987, ApJ 315, 469
Cardelli J.A., Clayton G.C., Mathis J.S., 1988, ApJ 329, L33
De Marchi G., Paresce F., 1995a, A&A 304, 202
De Marchi G., Paresce F., 1995b, A&A 304, 212
Djorgovski S.G., Meylan G., 1993, A&AS 182, 5015
Ferraro F.R., Carretta E., Bragaglia A., Renzini A., Ortolani S., 1997, MNRAS 286, 1012
Gould A., Bahcall J.N., Flynn C., 1997, ApJ 482, 913
Gratton R.G., Fusi Pecci F., Carretta E., et al., 1997, AJ 491, 749
Heasley J.N., Christian C.A., 1986, ApJ 307, 738
Holtzman J.A., Currows C.J., Casertano S., et al., 1995, PASP 107, 1065
Kroupa P., 1995, ApJ 453, 350
Kroupa P., Tout A.T., Gilmore G., 1993, MNRAS 262, 545
Johnson J.A., Bolte M., 1998, AJ 115, 693
Marconi G., Buonanno R., Carretta E., et al., 1998, MNRAS 293, 479
Mc-Clure R.., Vandenberg D.A., Smith G.H., et al., 1986, ApJ 307, L49
Mera D., Chabrier G., Baraffe I., 1996, ApJ 459, L87
Piotto G., Cool A.M., King I.R., 1997, AJ 113, 1345
Pont F., Charbonnel C., Lebreton Y., et al., 1997, Proceedings of the ESA Symposium Hipparcos - Venice '97, ESA SP-402
Pryor C., Smith G.H., Mc-Clure R.D., 1986, AJ 92, 138
Silvestri F., Ventura P., D'Antona F., Mazzitelli I., 1998, ApJ 509
Spitzer L., 1987, Dynamical evolution of globular clusters. Princeton University Press, Princeton, NJ
Stetson P.B., Harris W.E., 1988, AJ 96(3), 909
Tinney C., 1999, In: Gibson B.K., Axelrod T.S., Putman M.E. (eds.) The Third Stromlo Symposium: The Galactic Halo ASP Conf. dr. Vol. 165